

## Article

# Electrophysical Method for Identifying the Causes of Excessive Hydro Generator Vibration

Aleksei S. Karpov , Vera V. Yaroshevich, Galina P. Fastiy and Elizaveta I. Gubskaya

Northern Energetics Research Centre—Branch of the Federal Research Centre “Kola Science Centre of the Russian Academy of Sciences” (NERC KSC RAS), 14 Fersman Street, Apatity 184209, Russia; v.yaroshevich@ksc.ru (V.V.Y.); g.fastiy@ksc.ru (G.P.F.); e.gubskaya@ksc.ru (E.I.G.)

\* Correspondence: a.karpov@ksc.ru

**Abstract:** This article analyzes the operation of hydro generators based on the operation modes of a hydroelectric power plant operating in the Arctic zone of the Russian Federation. The main load of the hydropower plant is an aluminum smelter. The nonlinear load of the smelter is a powerful source of harmonic disturbances. This load produces current and voltage distortions not only in the electrical networks of the smelter but also in those of the city and in generating voltage busbars of the hydropower plant. As a consequence, higher harmonics cause additional losses in the supply networks and have a negative impact on the hydro generators’ condition. The article analyzes the influence of current impacts of the smelter load on the hydro generators under imbalanced conditions by estimating torsional and tangential vibrations emerging in the generators. The tangential forces of double frequency (100 Hz) have been shown to produce practically no significant vibration displacement when detuning the natural frequency of the basket-type end-winding parts. The values of vibration and surge displacement increase significantly in the near-resonance zone. The intense impact of superimposed surge currents has been shown to result in reduction in the hydraulic turbines’ service life and increase in frequency of repairs.

**Keywords:** hydropower plant; nonlinear load; hydro generator; torsional and tangential vibration



**Citation:** Karpov, A.S.; Yaroshevich, V.V.; Fastiy, G.P.; Gubskaya, E.I. Electrophysical Method for Identifying the Causes of Excessive Hydro Generator Vibration. *Appl. Sci.* **2023**, *13*, 9152. <https://doi.org/10.3390/app13169152>

Academic Editor: Dimitris Mourtzis

Received: 8 June 2023

Revised: 4 August 2023

Accepted: 8 August 2023

Published: 11 August 2023



**Copyright:** © 2023 by the authors. Licensee MDPI, Basel, Switzerland. This article is an open access article distributed under the terms and conditions of the Creative Commons Attribution (CC BY) license (<https://creativecommons.org/licenses/by/4.0/>).

## 1. Introduction

Renewable hydro energy power generation is one of the priorities of power engineering development. Hydroelectric power plants (HPPs) constitute a significant part of global power generation. HPPs are operated in strict compliance with legal requirements and regulatory standards [1–7]. A hydraulic turbine and a hydro generator are considered to be the most important and high-cost equipment of a hydroelectric power station. The service life of a hydro generator is 20–30 years [8].

Hydro generators are affected by nearby conversion units [9,10]. These can be a source of disturbances that can cause unfavorable resonance processes in turbine shaft trains. Because of the effect of control devices of a conversion unit, torsional vibration excitation occurs, leading to vibration problems, increase in damage frequency, and decrease in the service life of hydraulic turbines [11–13]. The authors discuss the causes of damage to hydraulic machines, turbines and the cost of such damage resulted from dynamic impacts at the conferences [14–22]. The Sayano-Shushenskaya HPP accident, the largest one in Russia, occurred in August 2009 and drew even more attention to this problem.

To investigate these phenomena, a cascade of hydropower plants located in the Arctic zone of Russia was considered.

## 2. A Brief Review of the Existing Investigations of the Causes of Hydro Generator Vibration

A large number of studies related to the urgent problem of hydro generator excessive vibration have been analyzed. Highlighted among the literature considered can be [23–30].

In [23], the effect of load current harmonics on vibration of three-phase generator is investigated. The results of laboratory experiments conducted show that the load nature strongly determines generator vibration. Higher load is revealed to result in higher generator vibration. Meanwhile, the higher the harmonic content of the load, the higher the vibration of a generator.

Song Z. et al. [24] analyzed torsional vibration parameters of a hydro generator set considering the coupling action of hydraulic and electromagnetic excitations. Electromagnetic vibration was investigated in terms of effects of excitation current and internal power angle on the amplitude of hydro generator torsional vibration. A finite element model of shaft system and method of vibration analysis to be applied to design and stable operation of hydro generator sets are proposed.

In [25], a 3D finite element model of the hydro generator shaft system established using ANSYS software is presented. The model proposed calculates the natural frequency of vibration and the critical speed of rotation. These parameters can be used to determine the dangerous resonance zone. The results obtained could provide a foundation for dynamic analysis and design or improvement of hydro generator set construction.

The study presented in [26] provides a foundation for guiding the structural design solutions and improvement of the hydro generator shaft system to avoid the resonance caused by external excitation sources, thereby ensuring the safety and stability of the hydro generator set operation. Consideration was given to the internal mechanism of shaft vibrations. Using a finite element model, the natural vibration characteristics and critical rotational speed of the shaft system were calculated. The results obtained formed the basis for the analysis and prediction of the possibility of resonance in hydro generators.

Guo D. et al. [27] studied the influence of the imbalanced magnetic pull (UMP) in a three-phase generator under a no-load condition caused by dynamic and static eccentricity of rotor on the rotor vibration.

Babic B. et al. [28] studied the correlation between vibration of generator guide bearings and magnetic imbalance of hydro generators. A method of magnetic monitoring that involves measuring the magnetic flux in the air gap in hydro generators was applied.

The research described in [29] consists in vibration analysis of a hydro generator that equips a Kaplan hydraulic turbine installed at a hydroelectric power plant in Romania. The results of vibration measurement for a no-load condition (without excitation and with excitation) and under-load condition are presented, with the measurement being conducted both before and after the hydro generator repair. An analysis of the influence of rotor magnetization state and hydraulic factors on the hydro generator vibration based on the experimental data obtained was performed.

In [30], the effect of hydraulic vibration on the stability of operation and service life of hydro generator sets was examined. To investigate nonlinear dynamic characteristics of the hydro generator resulting from hydraulic vibration, a nonlinear mathematical model of the hydro generator set was established using Lagrange equations.

These studies [23–30] described hydraulic, dynamic and magnetic effects on hydro generators. Our research was performed on an operating network on identification of the root causes of electrophysical effect on hydro generators, which defines its originality.

### 3. External Power Supply Diagram

The hydropower plant cascade under study operates mainly for the aluminum smelter (AS) needs. City networks are also among the consumers of the cascade. A simplified diagram of the AS external power supply is shown in Figure 1. The power source of the enterprise is its 10 kV switchgear (SWG). Electrical energy is supplied to the busbars of the 10 kV SWG by the busbars of the 10 kV generator switchgear (GSWG) of the HPP-I of the cascade and by the 110/10 kV substation (SS-I) of the power system.

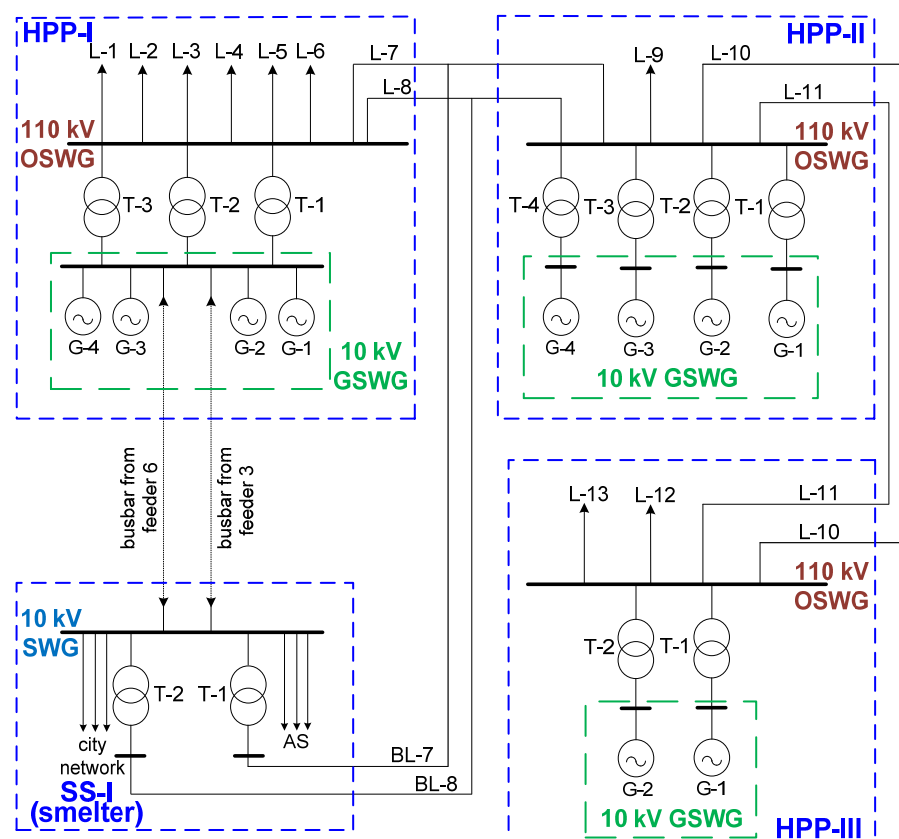


**Figure 1.** Simplified diagram of the smelter external power supply.

The smelter is connected to the 10 kV GSWG of the HPP-I by two busbars with the exact length of 1.44 and 1.36 km (feeder 3 and feeder 6, respectively). About 42 MW is transmitted through busbar 6 and 44 MW is transmitted through busbar 3. The maximum throughput of the busbars is designed for a current load of about 3000 A.

The energy-intensive equipment of the AS (conversion units of electrolysis row consisting of three-winding transformers, bridge rectifier units and saturable reactors) is powered by the 10 kV busbars of the SS-I substation. In this scheme, the 10 kV SWGR is the auxiliary switchgear of the hydropower plant.

The HPP-I has its own 110 kV outdoor switchgear (OSWG) to transmit power to the power grid. The 110 kV OSWG of the HPP-I is connected to the busbars of the 110 kV OSWG of the HPP-II of the cascade by 110 kV transmission lines (L-7 and L-8). The SS-I transformers (the smelter) are connected to the 110 kV network by two sub-branches, BL-7 and BL-8, of transmission lines L-7 and L-8, respectively. The HPP-I is the main power supply of the smelter. It has three 38.5 MW hydro generators and one 40 MW generator of the SV-655/110-32 type. According to the HPP-I operation service, at least three generators are constantly in operation.

Thus, the power supply system of the smelter has distinctive construction features compared to other similar enterprises. The main loads are the conversion units fed by various power supplies (the 10 kV busbars of the HPP-I and the 10 kV busbars of the 110/10 kV SS-I substation). This load affects all consumers of this network section, which is proven by recordings performed.

The recording of parameters of electrical energy flows and power quality indices was carried out on the busbars of the 10 kV GSWG of the HPP-I using certified recorders. During recording of steady-state mode parameters of electrical energy transmitted through busbars (electric power characteristic, dynamics of load variation recorded at time intervals of 1 min, limit values, etc.), voltage imbalance, current imbalance and harmonic content of voltage were obtained.

In addition, a specially designed metering complex was used. It allowed a long-term detailed recording of current impacts to be performed on hydro generators of the HPP-I, which allowed us to identify subharmonic and ultralow-frequency (UFL) components of current unrecorded before and transients with superposition of aperiodic component and pulses of current.

The description of the recording method is given in Appendix A. The experimental results obtained are given in Appendix B.

#### 4. Evaluation of Torsional and Tangential Vibrations

A negative impact on the HPP power equipment is due to distortion of both currents and voltages in the 10 kV busbars of the hydropower plant. This is possible when a hydro generator operates under imbalanced load conditions and forces that are uncharacteristic of normal operation emerge. For instance, an alternating electromagnetic moment of double synchronous frequency emerges [31], resulting in torsional vibration of the stator steel structures and the winding and the radial force of the magnetic pull of pole frequency emerging [32,33]. These forces excite radial core vibration. The vibration forces were evaluated in accordance with the methodology [32] given in Appendix C.

The estimation of the torsional  $T_0$  and radial  $F_0$  forces and the double amplitude of vibration (maximum displacement) in the indicated directions  $2W_1$  and  $2U_1$  for the option of imbalance—the negative sequence current  $i_2$ —are presented in Table 1. According to the data of the imbalance factor recording, a level of 2% (0.02 pu), which is actually not exceeded in the power supply system of the smelter, was taken.

**Table 1.** Vibration parameters of the elements of the 38.5 MW SV-655/110-32 type hydro generator when the imbalance factor is 0.02.

	Parameters	Symbol	Natural Frequency, Hz	Value, $\mu\text{m}$
Torsional vibration	Tangential core displacement amplitude	$2W_1$		1.5–2.2
	Absolute amplitude of basket-type end-winding part vibration	$A_1$	86 113	37.3–80.2 21.0–45.8
Radial vibration	Core vibration	$2U_1$		0.7–0.8

The linear tangential force  $T_0$  is 668 N/m when the imbalance current is 0.02 pu. The amplitude of the radial force  $F_0$  is 1040 N/m. As the stiffness values are assumed as a certain interval, the calculation results are presented as a range of variation.

As can be seen from the calculations above, the torsional forces and the amplitude of the tangential vibration as a first approximation are inversely proportional to the frequency of imbalanced current components and harmonics. The tangential forces do not produce significant vibration displacement when the 50 Hz negative sequence current is present, which contributes to the forces of double frequency (100 Hz) being produced if the natural frequency of the basket-type end-winding parts is sufficiently well tuned out from 100 Hz. As can be seen, there is an increase in the amplitude of the natural vibration of the end-winding parts at the natural frequency below 100 Hz. In the example considered, the maximum vibration reaches 80  $\mu\text{m}$  at the natural frequency of 86 Hz. The excitation conditions of the core tangential torsional vibration are far from being resonant: the vibration values are low, within 2  $\mu\text{m}$ . Thus, the existing load imbalance is safe for the hydro generators.

The superimposition of surge current impacts caused by the load of the smelter on the generators can be estimated by introducing the surge current impacts with an equivalent frequency  $\omega_E$ . Then, the total current  $I(t)$  is expressed as:

$$I(t) = I_p \cdot \cos(\omega t) \cdot [1 + I_A \cdot \exp(-t/\tau) \cdot \cos(\omega_E t + \varphi)] = I_p \cdot \cos(\omega t) + 0.5I_p I_A \exp(-t/\tau) \quad (1)$$

where  $I_p$  is the amplitude of the operating current and  $I_A$  is the amplitude of the surge current.

The surge impact is decomposed into positive and negative sequence waves with frequencies that differ by  $2\omega_E$  and a significant increase in the amplitude.

For the ULF current component with an amplitude of 100 A and frequency of 1.2–1.5 Hz, the linear tangential force  $T_0$  is 1340 N/m and the amplitude of the radial force  $F_0$  is 2080 N/m.

When surge currents with amplitude of 500–750 A are superimposed, the force impacts increase significantly. The linear tangential force  $T_0$  reaches 5040 N/m and the amplitude of the radial force  $F_0$  reaches 7800 N/m. The radial and tangential displacements increase accordingly. The surge displacement values are presented in Table 2.

**Table 2.** Vibration parameters of the elements of the 38.5 MW SV-655/110-32 hydro generator when the ULF current component and surge currents are superimposed.

	Parameters	Symbol	Value, $\mu\text{m}$
Torsional vibration	Amplitude of the tangential core displacement caused by the ULF current component	$2W_1$	4.8–8.3
	Tangential core displacement amplitude at surge currents	$2W_1$	95.2–117.0
Radial vibration	Core vibration caused by the ULF current components	$2U_1$	2.8–3.2
	Core shock vibration	$2U_1$	28.8–35.0

The impact considered has the following features.

The superimposition of the ULF component results in a slight vibration increase. However, there is a frequency shift in mechanical impacts that create unwanted frequencies and danger of their falling into the near-resonance zone. The current frequency shift is  $\pm 1.2$ – $1.5$  Hz; resulting in 48.5–49 Hz and 51.2–51 Hz magnetic fields being generated in the machine. The interaction with the field of fundamental frequency causes mechanical force emergence in the 98–102 Hz frequency range. Under near-resonance conditions, the vibration and surge displacement values  $2W_1$ ,  $2U_1$  increase significantly. If the natural frequency of the basket-type end-winding parts is beyond the 86–113 Hz range, the relative tangential vibration of the end-winding parts should not exceed 15–30  $\mu\text{m}$  under imbalanced conditions with the ULF components of current loads.

The surge current superimposition has a short-term nature. However, the displacement value reaches 35  $\mu\text{m}$  in the radial direction and 117  $\mu\text{m}$  in the tangential one, i.e., both exceed the acceptable level. As for hydro generators with a composite core, the core vibration should not exceed 30  $\mu\text{m}$  under balanced load conditions according to [7]. In addition, the recordings have shown such impacts to be of intense nature and able to repeat several times a minute. This contributes to the reduction in the hydraulic turbines' service life and confirms the cause of increased vibration noted during inspection and repair tests performed at the hydropower plant.

## 5. Conclusions

In this research, the recording of electrical energy parameters, power quality indices and the calculation of vibration forces were carried out to investigate electrophysical effects on hydro generators. The following conclusions can be deduced from the results obtained.

1. In the power supply scheme of the aluminum smelter, the powerful nonlinear load of the enterprise impacts negatively on the operation modes of the HPP-I power equipment in consequence of the distortion of currents and voltages in the 10 kV

busbars of the hydropower plant. Periodic routine testing of the HPP-I generators detected an increased level of stator core and upper-bracket vibration and increased level of shaft runout. This study has proved that this occurs when emerged in the generators are significant torsional and radial forces caused by the nonlinear load of the AS. The G-3 and G-4 generators operating through the F-6 busbar have the highest values of oscillation and vibration.

2. The effect of current impacts of the load of the smelter on the HPP-I hydro generators was analyzed by torsional forces, and tangential vibration emerged in the hydro generators' evaluation. The superimposition of negative sequence currents is shown to be a consequence of the load imbalance.
3. The tangential forces of double frequency (100 Hz) do not produce significant vibration displacement when the imbalance factor is less than 2%. The increase in the amplitude of the natural vibration of the basket-type end-winding parts occurs at natural frequency below 100 Hz. For instance, at a natural frequency of 86 Hz, the maximum oscillation reaches 80  $\mu\text{m}$ . When the tangential torsional vibration of the core is excited beyond the resonance frequency range, the vibration values are low, within 2  $\mu\text{m}$ .
4. The superimposition of the ultralow-frequency current component results in a slight increase in vibration up to 3  $\mu\text{m}$  in the radial direction and up to 8  $\mu\text{m}$  in the tangential one. In this case, a shift in the mechanical impact frequency, appearance of side frequencies, and increased danger of their falling into the near-resonance zone are observed. The values of vibration and surge displacement increase significantly under near-resonance conditions.
5. The cause of increased vibration noted during inspection and repair tests was identified. The study has shown that the surge current superimposition has a short-term nature, with the value of the vibration displacement exceeding the acceptable level. Such impacts have an intense nature, causing reduction in the hydraulic turbine service life and the need for more frequent repairs.

**Author Contributions:** Conceptualization, A.S.K., V.V.Y., G.P.F. and E.I.G.; Formal analysis, A.S.K., V.V.Y., G.P.F. and E.I.G.; Investigation, A.S.K., V.V.Y., G.P.F. and E.I.G.; Writing—original draft, A.S.K., V.V.Y., G.P.F. and E.I.G.; Writing—review & editing, A.S.K., V.V.Y., G.P.F. and E.I.G. All authors contributed equally to the study conception and design. All authors have read and agreed to the published version of the manuscript.

**Funding:** This research received no external funding.

**Institutional Review Board Statement:** Not applicable.

**Informed Consent Statement:** Not applicable.

**Data Availability Statement:** The data are not publicly available due to trade-secret protection.

**Conflicts of Interest:** The authors declare no conflict of interest.

## Appendix A. Description of Recording Method

To monitor power quality, Parma-type measuring instruments recommended by the Methodological Guidelines of the Ministry of Energy of the Russian Federation [34] were used.

Parma recorders are applied to solve the following practical problems:

- Recording of load curves of separate lines, electrical installations and an enterprise overall;
- Voltage graph recording at any point of an electric network, selection of voltage regulation mode at power supply centers and taps of the 6–10/0.4 kV transformers fitted with no-load tap changer;
- Power quality monitoring by “voltage deviation”, “frequency deviation”, and “negative sequence voltage ratio” indices;

- Assessment of power quality indices' compliance with the standards established and issuance of a compliance protocol;
- Establishment of poor-voltage quality causes (complaint investigation);
- Verification of correct operation of the automatic voltage regulation unit of transformers fitted with on-load tap changers;
- Adjustment of compensating devices to maintain power factor required.

The measurement errors of the instruments are given in Table A1.

**Table A1.** Main technical characteristics of the recorders during recording process.

Measured Values, $X$	Measurement Range, $X_{max}-X_{min}$	Average Time, s	Limits of Permissible Errors	
			Absolute Error, $\Delta X$	Relative Error, $\Delta X$
RMS voltage, V	$0.7 U_{Nom}-1.3 U_{Nom}$	60	–	$\pm 0.2\%$
Steady-state voltage deviation $\Delta U$ , %	–30+30	60	$\pm 0.2$	–
Steady-state fundamental RMS voltage $U_{(1)}$ , V	$0.7 U_{Nom}-1.3 U_{Nom}$	60	–	$\pm 0.2\%$
Steady-state deviation of fundamental RMS voltage $\Delta U_{(1)}$ , %	–30+30	60	$\pm 0.2$	–
Frequency $f$ , Hz	45–55	20	$\pm 0.02$	–
Frequency deviation $\Delta f$ , Hz	–5+5	20	$\pm 0.02$	–
Negative sequence voltage ratio $K_{2U}$ , %	0–30	3	$\pm 0.3$	–
Zero sequence voltage ratio $K_{0U}$ , %	0–30	3	$\pm 0.3$	–
Total voltage harmonic distortion $K_U$ , %	0–30	3	When $K_U < 1\% \pm 0.1\%$	When $K_U > 1\% \pm 10\%$
Factor of $n^{\text{th}}$ voltage harmonic component $K_{U(n)}$ , $n = 2 \dots 40$ , %	0.05–30.00	3	When $K_{U(n)} < 1\% \pm 0.05\%$	When $K_{U(n)} > 1\% \pm 5\%$
Voltage swell factor $K_{Swell}$ , %	$D^{-1}-1.3$	–	$\pm 2.2/U_{Nom}$	–
Voltage dip depth $\Delta U_{Dip}$ , %	$dU_{Under Limit}^2-100$	–	$\pm 220/U_{Nom}$	–
Dip duration $\Delta t_{Dip}$ , ms	10–59,960	–	When $\Delta t_{Dip} < 20 \text{ s} \pm 10 \text{ ms}$ When $\Delta \Delta t_{Dip} > 20 \text{ s} \pm 20 \text{ ms}$	–
Swell duration $\Delta t_{Swell}$ , ms	40–59,960	–	When $\Delta t_{Swell} < 20 \text{ s} \pm 10 \text{ ms}$ When $\Delta t_{Swell} > 20 \text{ s} \pm 20 \text{ ms}$	–
Astronomical time	–	–	$\pm 1 \text{ s/day}$	–
Maximum time of continuous recording				10,080 min
Nominal RMS voltage value $U_{Nom}$ , V				45–400

Recording sensitivity of measured value deviation according to the set point of tolerance values does not exceed the limits of permissible recorder errors when measuring the corresponding measured values. <sup>1</sup>  $D = 1 + dU_{Over Limit}/100$ , where  $dU_{Over Limit}$  refers to the set permissible voltage over-deviation. <sup>2</sup>  $dU_{Under Limit}$  refers to the set permissible voltage under-deviation.

While taking recordings using Parma recorders, data sufficient to study negative effects of the smelter load appeared to be impossible to obtain. This is due to the automated processing technique inherent to the recorders. During processing, the information is displayed with a time interval of 1 min, which does not allow subharmonics or interharmonics to be identified. Meanwhile, it is impossible to accumulate detailed information over a longer time interval because of the internal memory limited capacity. Therefore, to record transients and obtain more detailed information, a metering complex developed at the was additionally used. The metering complex (MC) based on a PC, an L-card ADC/DAC external module and a sensor unit (SU) enables continuous recording through 10 channels

with time sampling from 100  $\mu$ s per channel. The sensor unit has four voltage sensors and six current sensors. All LEM sensors are based on the Hall effect. A block diagram of the metering complex is shown in Figure A1.

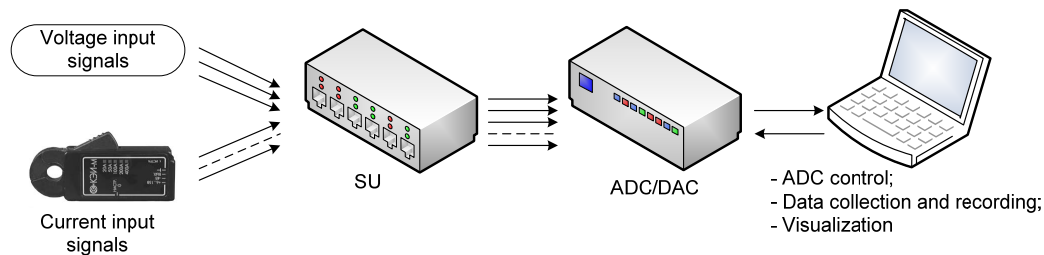


**Figure A1.** Block diagram of the metering complex.

The experiment was carried out on feeders 3 and 6 near the 10 kV generator voltage busbars of HPP-I in several stages in order to obtain data at different times of the year.

A diagram of connection of a metering system, which includes Parma recorders and the metering complex, to voltage transformers (VTs) and current transformers (CTs) is shown in Figure A2.

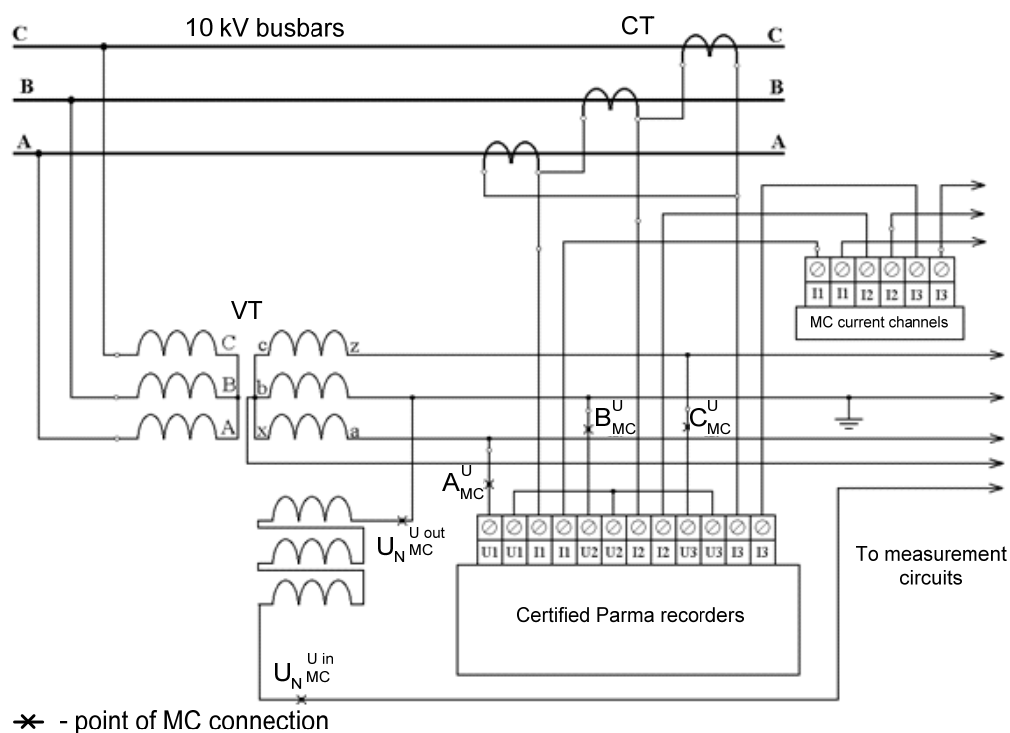


**Figure A2.** Diagram of connection of the metering system to network.

During measurements performed using a digital oscilloscope and LabView devices to record data on a computer hard drive, channels of voltage measurement were connected to MC channels of voltage measurement in parallel (Figure A2). During recording of currents, MC current sensors were connected to the break of series input circuits of Parma recorders and those of relay protection and automation devices. The input circuits of the recorder are equipped with LEM current sensors based on the Hall effect, which enable complete galvanic isolation and high accuracy of measurements within a given frequency range. The input parameters of the metering system were monitored, i.e., the total input impedance was less than 0.2 ohms.

## Appendix B. Results of Steady-State Mode Recording

The research performed included recordings of steady-state processes and transients in the 10 kV GSWG busbars of the HPP-I and higher harmonics emitted by the load of the aluminum smelter in the supply network. The recordings were carried out by using certified Parma recorders and the metering complex purpose-designed for long-term continuous recording of processes across several channels. Continuous recording was performed in several stages in compliance with the standard requirements.

The results of recording were obtained as archived numerical data that can be presented as daily and hourly graphs, histograms with different time scales, or in tabular form and in protocols. Detailed experiment protocols describing all electrical parameters are the property of the customer of these works, being protected by a nondisclosure agreement (NDA), so the positioning of the protocols with a specific enterprise is impossible. However, observations of the physical processes occurring in the high-voltage networks under study are the subject of great interest for the scientific community to study and optimize the operation of hydro generators, regardless of location in the world. The most interesting results are presented in this article.

From the results of recordings of steady-state processes, parameters of electrical energy flows and power quality indices, the following characteristics of the operating conditions of the HPP-I hydro generators that have direct low-impedance connection to facilities of the smelter have been deduced.

1. Voltage deviations on both busbars are 1.3–6.7%. The maximum deviations exceed 6–7%, being systematic (mathematical expectation is greater than 4%), indicating the presence of surge current impact and the lack of load control effect.
2. The voltage imbalance ratio is less than 2%, indicating the load is evenly distributed among the phases.
3. The recording data (with output in 1 min) identifies current variations of up to 500 A with an intensity of up to seven variations per hour. According to the detailed recording data, the variation in current loads has a surge nature. The rate of current variation reaches 750 A/s on the front edge, with this being about 500 A/s on the back edge. The surge impacts have an irregular but systematic nature, repeating multiple times within 1 min.
4. The current impact on the hydro generators has ULF components with frequency of 1.2–1.5 Hz and about 0.1 Hz permanently superimposed.
5. The voltage harmonic distortion exceeds the permissible values specified by the standard. Exceeding the maximum permissible value in feeder 6 of the 10 kV GSWG of the HPP-I are the 11th, 13th, 23rd and 25th harmonics, this being of systematic nature. This indicates high emission of higher harmonics into the supply network in practice. The reduction in harmonics is mainly enabled by a shunt effect of the hydro generator's low impedance.

The recordings of transients emitted in the 10 kV GSWG busbars of the HPP-I and the corresponding current loads showed an aperiodic component with amplitude up to 1.3–1.6 kA and current pulses of 0.5 kA to 3.9 kA, with duration less than 0.1 ms being superimposed. The rate of the aperiodic component variation on the front edge is up to 20 kA/s, while the aperiodic component duration on the back edge does not exceed 0.3 s. The equivalent frequency of the current impact is about 2 Hz.

## Appendix C. Description of Vibration Force Calculation

The radial component of the linear force  $F_0$  is proportional to the induction B in the air gap, which can be represented as the waves of positive  $B_1$  and negative  $B_2$  sequence:

$$F_0 = \frac{B_1 \cdot B_2 \cdot l}{2\mu_0} \cdot \cos(2 \cdot \omega \cdot t - \gamma_2) \quad (\text{A1})$$

where  $l$  refers to the active length of the machine,  $\gamma_2$  is a certain phase angle, and  $t$  stands for time.

The torsional vibration of stator steel structures is caused by the impact of an alternating electromagnetic moment  $M$  of frequency  $2\omega$ . Under imbalanced load conditions, the relative value of the moment  $M$  is approximately equal to the negative sequence current  $i_2$  (pu). As a result, the tangential force can be expressed as:

$$T_0 = \frac{M_n \cdot i_2}{2\pi \cdot R_1^2} \tag{A2}$$

where  $M_n$  is the nominal moment of generator and  $R_1$  is the core radius.

The relationship between tangential forces and displacement is described by the following system of two equations:

$$\begin{cases} -4\omega^2 m_1 W_1 + k_{t1} \cdot (W_1 - W_2) = \frac{M}{2\pi \cdot R_1^2} = T_0 \\ -4\omega^2 m_2 W_2 + k_{t1} \cdot (W_2 - W_1) + k_{t2} W_2 = 0 \end{cases} \tag{A3}$$

Here,  $W_1$  and  $W_2$  are the amplitudes of tangential displacements of the core and the housing, respectively;  $m_1$  and  $m_2$  are the linear masses of the core (along with the winding) and the housing, respectively; and  $k_{t1}$  and  $k_{t2}$  are the stiffnesses of the connection between the core and the housing and that between the housing and the foundation, respectively, in the tangential direction.  $T_0$  refers to the linear tangential force corresponding to the moment  $M$ .

Hence, the amplitude of the tangential core displacement is expressed as:

$$W_1 = \frac{T_0}{-4\omega^2 m_1 + \frac{k_{t1} \cdot (k_{t2} - 4\omega^2 m_2)}{k_{t1} + k_{t2} - 4\omega^2 m_2}} \tag{A4}$$

To estimate the vibration of the end-winding parts of stator winding in the first approximation, it is assumed that there is one degree of freedom for the basket-type end-winding parts, i.e.,

$$4\omega^2 m_0 A - k_0(A - W_1) = 0 \tag{A5}$$

where  $m_0$  refers to the equivalent mass and  $k_0$  stands for the equivalent stiffness. The absolute ( $A$ ) and relative ( $A - W_1$ ) amplitudes of oscillation of the basket-type end-winding parts are expressed as:

$$A = \frac{W_1}{1 - 4\omega^2 \cdot \omega_0^{-2}} \tag{A6}$$

$$A - W_1 = \frac{4\omega^2 \cdot \omega_0^{-2}}{1 - 4\omega^2 \cdot \omega_0^{-2}} \cdot W_1 \tag{A7}$$

where  $\omega_0 = \sqrt{k_0/m_0}$  is the frequency of natural vibration of the basket-type end-winding parts when these are under kinematic excitation.

Under imbalanced load conditions, the radial forces of the magnetic pull and the magnetic vibration excited by these forces are estimated considering that the linear force of the magnetic pull  $F(\varphi, t)$  is equal to:

$$F(\varphi, t) = \frac{1}{2\mu_0} \cdot [B(\varphi, t)]^2 \cdot l \tag{A8}$$

where  $B(\varphi, t) = B_1 \cdot \cos(p \cdot \varphi - \omega \cdot t) + B_2 \cdot \cos(p \cdot \varphi + \omega \cdot t - \gamma_2)$  is the induction in the air gap presented as the rotating waves of positive ( $B_1$ ) and negative ( $B_2$ ) sequences,  $\varphi$  refers to the angular coordinate,  $p$  refers to the number of pole pairs, and  $\mu_0$  stands for the vacuum permeability.

It is assumed that  $B_1 = B_n$  and  $B_2 = B_n x_2 i_2$ , where  $B_n$  is the nominal induction in the air gap and  $x_2$  refers to the negative sequence reactance expressed in pu.

Hence, the amplitude of the radial force  $F_0$  can be determined by the following expression:

$$F_0 = \frac{1}{2\mu_0} \cdot B_n^2 \cdot x_2 \cdot i_2 \cdot l = 4 \cdot 10^5 \cdot B_n^2 \cdot x_2 \cdot i_2 \cdot l \quad (\text{A9})$$

Introducing the stiffnesses of the connection between the core and the housing  $k_{r1}$  and of that between the housing and the foundation  $k_{r2}$  in the radial direction and also the amplitudes of radial displacements of the core  $U_1$  and the housing  $U_2$ , the following system of equations is obtained:

$$\begin{cases} F_0 = -4\omega^2 m_1 U_1 + k_1 U_1 + k_{r1}(U_1 - U_2) \\ 0 = -4\omega^2 m_2 U_2 + k_2 U_2 + k_{r1}(U_2 - U_1) + k_{r2} U_2 \end{cases} \quad (\text{A10})$$

The values  $k_1$  and  $k_2$  represent the intrinsic linear stiffnesses of the core and the housing for purely radial displacement, both being determined by the cross-sectional area of the core  $S_1$  and that of the housing  $S_2$ , the equivalent elastic modulus of the core  $E_1$  and that of the housing  $E_2$ , the radius of the core  $R_1$  and that of the housing  $R_2$ , i.e.,  $k_1 = E_1 S_1 / R_1$ ,  $k_2 = E_2 S_2 / R_2$ .

As a result, the following expression of the radial core vibration is obtained:

$$U_1 \cong F_0 \cdot \left[ -4\omega^2 m_1 + k_1 + \frac{k_{r1}(k_2 + k_{r2} - 4\omega^2 m_2)}{k_{r1} + k_{r2} + k_2 - 4\omega^2 m_2} \right]^{-1} \quad (\text{A11})$$

In further calculations, the  $k_{t1} \approx k_{r1} \approx (5 \dots 10) \times 10^8$  N/m and  $k_{t2} \approx (5 \dots 10) \times 10^8$  N/m,  $k_{r2} \approx 2 \times 10^8$  N/m values are assumed according to the data of [35–37], respectively.

## References

1. GOST R 55260.1.9-2013; Hydro Power Plants. Part 1–9. Hydraulic Structures of Hydropower Stations. Safety Requirements under Operation. Federal Agency for Technical Regulation and Metrology: Moscow, Russia, 2013.
2. STO 17330282.27.140.015-2008; Hydroelectric Power Plants. Organization of Operation and Maintenance. Standards and Requirements. RAO UES of Russia: Moscow, Russia, 2008.
3. STO 17330282.27.140.007-2008; Technical Systems of Hydroelectric Power Plants. Organization of Operation and Maintenance. Standards and Requirements. RAO UES of Russia: Moscow, Russia, 2008.
4. 13373-2:2005; Condition Monitoring and Diagnostics of Machines—Vibration Condition Monitoring—Part 2: Processing, Analysis and Presentation of Vibration Data. International Organization for Standardization: Geneva, Switzerland, 2016.
5. GOST R ISO 7919-1-99; Mechanical Vibration of Non-Reciprocating Machines. Measurements on Rotating Shafts and Evaluation Criteria. General Guidelines. Russian Federation Gosstandart: Moscow, Russia, 1999.
6. GOST ISO 10816-1-97; Mechanical Vibration. Evaluation of Machine Vibration by Measurements on Non-Rotating Parts. Part 1. General Guidelines. Inter-Governmental Council on Standardization, Metrology, and Certification: Moscow, Russia, 1997.
7. GOST 5616-89; Water-Wheel Type Generators and Motor-Generators. General Specifications. USSR National Committee on Standards: Moscow, Russia, 1989.
8. Stone, G.C.; Boulter, E.A.; Culbert, I.; Dhirani, H. *Electrical Insulation for Rotating Machines: Design, Evaluation, Aging, Testing and Repair*, 1st ed.; Wiley: Hoboken, NJ, USA, 2004.
9. Berkh, I.M.; Koshkarev, A.V.; Smolovik, S.V. The Study of Operation Conditions of Turbine Generators near Powerful Conversion Units. *Power Plants* **1990**, *3*, 23–27.
10. Rubisov, G.V.; Sigaev, V.E. Computational Method to Analyze Torsional Vibration of a Turbine-Set Shaft Train. *Electr. Eng.* **1986**, *1*, 27–31.
11. Konidaris, D.N.; Tegopoulos, J.A. Investigation of Oscillatory Problems of Hydraulic Generating Units Equipped with Francis Turbines. *IEEE Trans. Energy Conv.* **1997**, *12*, 419–425. [[CrossRef](#)] [[PubMed](#)]
12. Vasiliev, Y.S.; Petrenya, Y.K.; Georgievskaya, E.V. Lifetime of Hydro Turbines: A Review of Foreign Literature. *St. Petersburg. Polytech. Univ. J. Eng. Sci. Technol.* **2017**, *23*, 184–204. [[CrossRef](#)]
13. Li, Y.; Huang, Z.; Li, H.; Song, G. Analysis of Nonlinear Dynamic Characteristics of a Mechanical-Electromagnetic Vibration System with Rubbing. *Appl. Sci.* **2019**, *9*, 4612. [[CrossRef](#)]
14. Frunzäverdel, D.; Muntean, S.; Mărginean, G.; Câmpian, V.; Marşavina, L.; Terzi, R.; Şerban, V. Failure Analysis of a Francis Turbine Runner. *IOP Conf. Ser. Earth Environ. Sci.* **2010**, *12*, 012115. [[CrossRef](#)]
15. Gammer, J.H.; Etter, S. Cracking of Francis Runners during Transient Operation. *Int. J. Hydropower Dams* **2008**, *15*, 81–84.
16. Zouhar, J.; Obrovsky, J.; Feilhauer, M.; Skotak, A. Case Study and Numerical Analysis of Vibration and Runner Cracks for the Lipno I Hydroelectric Project. *IOP Conf. Ser. Earth Environ. Sci.* **2016**, *49*, 072011. [[CrossRef](#)]

17. Sick, M.; Oram, C.; Braum, O.; Nenneman, B.; Coutu, A. Hydro Projects Delivering Regulating Power: Technical Challenges and Cost of Operation. In Proceedings of the Hydro, Innsbruck, Austria, 7–9 October 2013.
18. Favrel, A.; Landry, C.; Müller, A.; Avellan, F. Experimental Identification and Study of Hydraulic Resonance Test Rig with Francis Turbine Operating at Partial Load. *IOP Conf. Ser. Earth Environ. Sci.* **2012**, *15*, 062064. [[CrossRef](#)]
19. Sabourin, M.; Thibault, D.; Bouffard, D.A.; Lévesque, M. New Parameters Influencing Hydraulic Runner Lifetime. *2010 IOP Conf. Ser. Earth Environ. Sci.* **2010**, *12*, 012050. [[CrossRef](#)]
20. Poll, H.G.; Zanutto, J.C.; Ponge-Ferreira, W. Hydraulic Power Plant Machine Dynamic Diagnosis. *Shock Vib.* **2006**, *13*, 409–427. [[CrossRef](#)]
21. Trivedi, C.; Gandhi, B.; Michel, C. Effect of Transients on Francis Turbine Runner Life: A Review. *J. Hydraul. Res.* **2013**, *51*, 121–132. [[CrossRef](#)]
22. Radchenko, V.V. System Requirements to the Efficiency of Hydroelectric Power Stations. *Electr. Eng. Power Eng.* **2018**, *3*, 22–29. [[CrossRef](#)]
23. Kastawan, I.M.W. Effect of Load Current Harmonics on Vibration of Three-Phase Generator. *MATEC Web Conf.* **2018**, *197*, 11023. [[CrossRef](#)]
24. Song, Z.; Liu, Y.; Guo, P.; Feng, J. Torsional Vibration Analysis of Hydro-Generator Set Considered Electromagnetic and Hydraulic Vibration Resources Coupling. *Int. J. Precis. Eng. Manuf.* **2018**, *19*, 939–945. [[CrossRef](#)]
25. Bai, B.; Zhang, L.; Guo, T.; Liu, C. Analysis of Dynamic Characteristics of the Main Shaft System in a Hydro-Turbine Based on ANSYS. *Procedia Eng.* **2012**, *31*, 654–658. [[CrossRef](#)]
26. Wang, W.; Shang, Y.; Yao, Z. A Predictive Analysis Method of Shafting Vibration for the Hydraulic-Turbine Generator Unit. *Water* **2022**, *14*, 2714. [[CrossRef](#)]
27. Guo, D.; Chu, F.; Chen, D. The Unbalanced Magnetic Pull and Its Effects on Vibration in a Three-Phase Generator with Eccentric Rotor. *J. Sound Vib.* **2002**, *254*, 297–312. [[CrossRef](#)]
28. Babic, B.; Kartalovic, N.; Marinkovic, S.; Misovic, D.; Teslic, D.; Milosavljevic, Z.; Nikolic, A. Correlations between Magnetic and Vibration Measurements on Hydro Generators. In Proceedings of the 2nd International Conference on Intelligent Control, Modelling and Systems Engineering (ICMS'14), Cambridge, MA, USA, 29–31 January 2014; pp. 171–175.
29. Hațegan, C.; Pădureanu, I.; Jurcu, M.; Nedeloni, M.D.; Hamat, C.O.; Chioncel, C.P.; Trocaru, S.; Vasile, O.; Bădescu, O.; Miciuc, D.; et al. Vibration Analysis of a Hydro Generator for Different Operating Regimes. *IOP Conf. Ser. Mater. Sci. Eng.* **2017**, *163*, 012030. [[CrossRef](#)]
30. Zhuang, K.; Huang, S.; Fu, X.; Chen, L. Nonlinear Hydraulic Vibration Modeling and Dynamic Analysis of Hydro-Turbine Generator Unit with Multiple Faults. *Energies* **2022**, *15*, 3386. [[CrossRef](#)]
31. Nadtochiy, V.M.; Tsvetkov, V.A. Forces and Vibration in Hydro Generators during Their Operation in Unbalanced Modes. *Electr. Technol.* **1989**, *9*, 77–88.
32. Ter-Gazaryan, G.N. *Asymmetric Modes of Synchronous Machines*; Energy: Moscow, Russia, 1969.
33. Xu, S. Magnetic Vibration of Hydro Generator Stator Core Due to Rotor Eccentricity, Rotor Non-Circularity and Negative-Sequence Current. *Electra* **1983**, *86*, 77–88.
34. *Methodological Guidelines of the Ministry of Energy of the Russian Federation*; Energoservice: Moscow, Russia, 2001.
35. Kislitsky, B.V. Computational and Experimental Studies of the Stress State of Steel Structures of the Composite Stator of Hydro Generators. *Sov. Electr. Eng.* **1985**, *7*, 53–62.
36. Petrov, Y.V. Natural Frequencies of Stators of Large Hydro Generators. *Sov. Electr. Eng.* **1980**, *8*, 5–8.
37. Petrov, Y.V. Magnetic Vibration of the Hydro Generator Stator with Revolving Frequencies. *Trans. All-Union Res. Inst. Power Eng.* **1977**, *53*, 11–19.

**Disclaimer/Publisher's Note:** The statements, opinions and data contained in all publications are solely those of the individual author(s) and contributor(s) and not of MDPI and/or the editor(s). MDPI and/or the editor(s) disclaim responsibility for any injury to people or property resulting from any ideas, methods, instructions or products referred to in the content.